Theoretical Chemistry Accounts (2023) 142:111
https://doi.org/10.1007/s00214-023-03052-2

RESEARCH

DFT study of the condensation products of 2-chloro-3-formylquinolines with o-aminophenol, o-aminothiophenol and o-phenylenediamine

Nabila Benabila[1,2] · Hafida Merouani[2,3] · Nadjia Latelli[1,2] · Abd Alghani May[4] · Christophe Morell[5] · Lynda Merzoud[5] · Henry Chermette[5]

Received: 22 December 2022 / Accepted: 8 September 2023

Abstract
The reaction mechanism for the synthesis of quinoline-fused benzo/dia/oxa/thia/zepins is investigated using the DFT/B3LYP/6-31G(d) method. DFT conceptual reactivity indices analysis allows classification of o-aminophenol (2, X = O), o-aminothiophenol (2, X = S) and o-phenylenediamine (2, X = N) and R-substituted 2-chloroquinoline-3-carbaldehydes (1 ac) as strong electrophiles, suggesting a polar process. Besides, Parr functions and Fukui indices predict the most reactive sites for observed experimentally product formation, in agreement with the dual descriptor analysis. In the energy aspect, there is no effect of the R (R = CH_3, OCH_3) substituent on the thermodynamic quantities, whereas the substitution of the X has a remarkable effect. The products (4a–c, X = N) are the most stable, and their cyclizations are the easiest. An extended analysis was performed using the activation strain model/energy decomposition analysis ASM/EDA model. The obtained results indicate that the orbital interaction and electrostatic stabilizations are the principal factors favoring the reaction with X = N. Topological analysis of the electron localization function (ELF) of the bending point structures along the reaction path indicates that the reaction occurs via a non-concerted two-step mechanism.

Keywords Benzo/oxa/thia/dia/zepines-fused quinolone · DFT · ELF · ASM/EDA model

1 Introduction

In the uninterrupted development of heterocyclic chemistry, now indispensable in organic synthesis, the heterocycle constitutes the basic skeleton in a wide variety of compounds of chemical, biological interest pharmacological and industrial interest [1, 2]. Heterocyclic compounds constitute an important class of organic molecules [3, 4] and constantly attract the interest of synthetic organic chemists. The search for new methods of heterocycles synthesis is crucial for the development of new compounds with biological potential to satisfy an ever-increasing demand for original molecules, and it is

✉ Hafida Merouani
h.merouani@univ-batna2.dz; merouani_hafida@yahoo.fr

✉ Henry Chermette
henry.chermette@univ-lyon1.fr

Nabila Benabila
nabila.bennabila@univ-msila.dz

Nadjia Latelli
nadjia.latelli@univ-msila.dz

Abd Alghani May
may01dz@yahoo.fr

Christophe Morell
christophe.morell@univ-lyon1.fr

Lynda Merzoud
lynda.merzoud@isa-lyon.fr; lyndamerzoud@gmail.com

[1] Faculty of Science, Department of Chemistry, University of Msila, BP 166 Ichbilia, 28000 M'sila, Algeria

[2] Laboratoire Chimie Des Matériaux Et Des Vivants: Activité, Réactivité, Université El-Hadj, Lakhdar Batna1, 05001 Batna, Algeria

[3] Faculty of Technology, Common Core Department, University of Ben Boulaid Batna 2, Batna, Algeria

[4] Département de Chimie, Université Frères Mentouri, Route de Ain El Bey, 25017 Constantine, Algeria

[5] University of Lyon, Université Lyon 1 et CNRS UMR 5280, Institut des Sciences Analytiques, 5 rue de la Doua, 69100 Villeurbanne, France

Published online: 09 October 2023

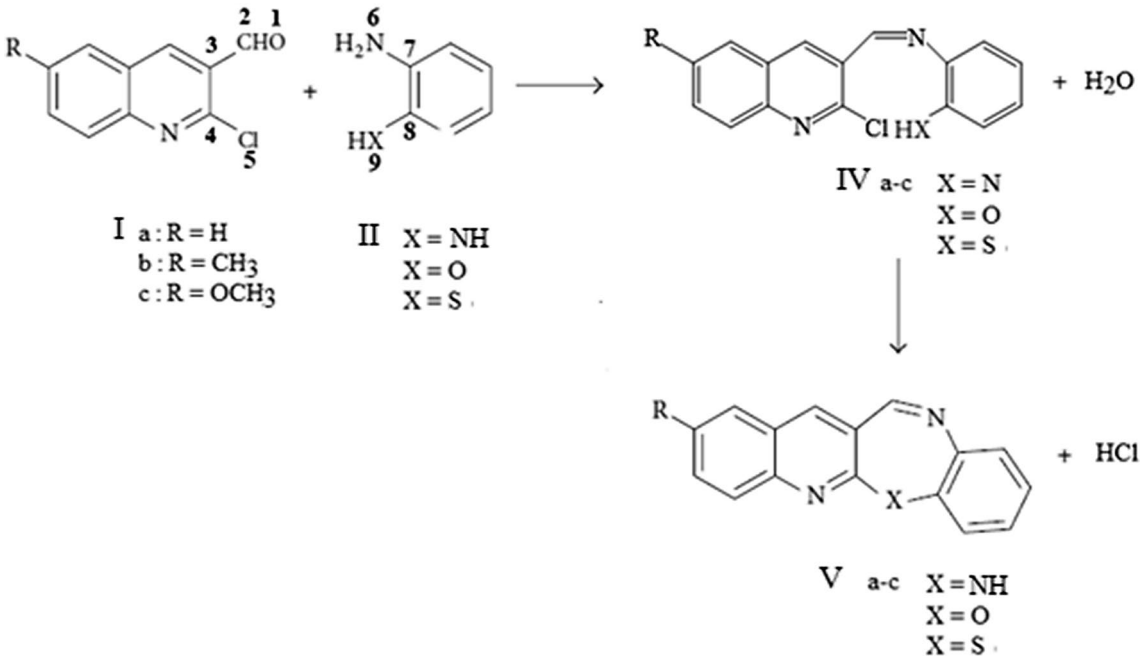

Scheme 1 The condensation of 2 chloroquinoline-3-carbaldehydes (**I** a-c) with o-phenylenediamine (**II**, X = NH), o-aminophenol (**II**, X = O) and o-aminothiophenol (**II**, X = S)

essential to develop new reaction sequences that are more efficient and selective within a limited number of operations.

Nitrogen heterocycles are of particular interest because they constitute an important class of natural and synthetic products, many of them exhibit important biological activities and unique electrical and optical properties [5–7]. Although condensed seven-membered heterocycles have been the subject of many synthetic studies considering their pharmacological properties, little work has been done on the preparation of tetracyclic derivatives. This is particularly the case in the area that interests us, namely the synthesis of benzoquinoline derivatives.

As new examples of synthetic applications of 2-chloro-3-formylquinolines, several condensed heterocycles have been prepared, among them the synthesis of quinoline-fused benzodiazepines (**V** a-c, X = NH) was attempted for the first time, by Bhanumathi et al. [8], through a reaction of 2-chloro-3 formylquinoline (**I** a-c) with o-phenylenediamine (**II**, X = NH) (Scheme 1) to study their pharmacological activity.

The condensation of 2 chloroquinoline-3-carbaldehydes (**I** a-c) with o-aminophenol (**II**, X = O) [9] and o-aminothiophenol (**II**, X = S) [10] in NN-dimethylformamide (DMF) in the presence of dry potassium carbonate under the conditions adopted by Nielsen and Pedersen [11], quantitatively yielded intermediate imines (**IV** a-c), which were then cyclized with high yields to quino-benzoxazepines (**V** a-c, X = O) and quino-benzothiazepine (**V** a-c, X = S), respectively (Scheme 1), as the main products. The reactions were carried out at room temperature, and the intermediate imines could not be isolated.

For a better understanding of the factors controlling the reaction, a theoretical approach is carried out by density functional theory (DFT). The activation strain model and energy decomposition analysis (ASM/EDA) allow monitoring the physical factors controlling the kinetics of these reaction. More details about ASM and EDA are given in Sect. 3.4.1.

2 Methodology and equations of the used calculation

All geometries were optimized at the B3LYP/6-31G (d) [12, 13] computational level using the Gaussian 09W [14] program. The existence of the transition state was confirmed by the presence of one and only one imaginary frequency, which leads to the formation of the corresponding product. The IRC calculation [15, 16] was carried out in order to verify that the TS is well connected to the two minima (reactants and product). The enthalpy and the free enthalpy of each stationary point were evaluated at $T = 298.15$ K and at $P = 1$ atm.

The reactivity of molecules and the mechanisms of reactions are first studied through the analysis of the wave function, which defines the quantum state of the molecular system. For example, the theory of Frontier Orbitals [17, 18] has been very effective in understanding the regioselectivity of organic

reactions, through the study of phase overlap or phase opposition between the highest occupied orbital of the nucleophile and the lowest vacant orbital of the electrophile. Electrophilic power is therefore defined as the energy stabilization due to charge transfer [19–21]:

$$\boldsymbol{\omega} = \frac{\boldsymbol{\mu}^2}{2\boldsymbol{\eta}} \tag{1}$$

The electronic chemical potential μ and the global hardness η can be calculated from the energies of the frontier molecular orbitals $\varepsilon_{\mathrm{HOMO}}$ et $\varepsilon_{\mathrm{LUMO}}$ [22–24]:

$$\mu = (\boldsymbol{\varepsilon_{HOMO}} + \boldsymbol{\varepsilon_{LUMO}})/2 \tag{2}$$

$$\boldsymbol{\eta} = \boldsymbol{\varepsilon_{LUMO}} - \boldsymbol{\varepsilon_{HOMO}} \tag{3}$$

In 2008, Domingo's group proposed an empirical (relative) nucleophilicity index (N) based on the energy (HOMO) obtained by the Kohn–Sham method [25]. This index is defined as follows [26, 27]:

$$\boldsymbol{N} = \boldsymbol{\varepsilon_{HOMO}}(\boldsymbol{Nu}) - \boldsymbol{\varepsilon_{HOMO}}(\boldsymbol{TCE}) \tag{4}$$

where Nu means the nucleophile reactant.

Note that the scale of nucleophilicity is referenced against the tetracyanoethylene (TCE) molecule taken as a reference because it exhibits the lowest HOMO energy in a large series of molecules.

The condensed form of the Fukui functions corresponding to the site k in a molecule with N electrons was proposed by Yang and Mortier [28]:

$$f_k^+ = \left[q_k(N+1) - q_k(N)\right] \quad \text{for a nucleophilic attack} \tag{5}$$

$$f_k^- = \left[q_k(N) - q_k(N-1)\right] \quad \text{for an electrophilic attack} \tag{6}$$

$q_k(N)$: Electronic population of atom k in the neutral molecule.

$q_k(N+1)$: Electronic population of atom k in the anionic molecule.

$q_k(N-1)$: Electronic population of atom k in the cationic molecule.

It has been shown, for reactions controlled by the frontier orbitals, that high values of the Fukui indexes mean a high reactivity of the site [29].

In 2013, Domingo [30, 31] proposed the Parr functions P(r) that characterize the change in spin electron density that occurs during the process of GEDT (Global Electron Density Transfer) from the nucleophile to the electrophile.

$$P^-(r) = \rho_s^{rc}(r) \quad \text{for an electrophilic attack} \tag{7}$$

$$P^+(r) = \rho_s^{ra}(r) \quad \text{for a nucleophilic attack} \tag{8}$$

where $\rho_s^{rc}(r)$ and $\rho_s^{ra}(r)$ are the atomic spin densities (ASD) of the atom r of the cation radical and the anion radical, respectively, of the molecule studied.

The spin densities of the N + 1/N-1 systems have been shown to be good approximations for the nucleophilic and electrophilic Fukui functions. Thus, the dual descriptor is calculated by the difference between the Fukui functions f^+ and f^- [32, 33].

$$\Delta\boldsymbol{f}(\boldsymbol{r}) = \boldsymbol{f}^+(\boldsymbol{r}) - \boldsymbol{f}^-(\boldsymbol{r}) = \boldsymbol{\rho_{LUMO}}(\boldsymbol{r}) - \boldsymbol{\rho_{HOMO}}(\boldsymbol{r}) \tag{9}$$

Since the dual descriptor encapsulates both electrophilic and nucleophilic reactivity tendencies in a single value, it is a powerful descriptor because chemical reactions often involve a complex interplay between these two types of reactivity. Then, the use of the dual descriptor Δf (r) allows an unambiguous prediction of the most reactive site toward an electrophilic or nucleophilic attack.

The Electron Localization Function (ELF) is a mathematical and conceptual tool used in the field of theoretical chemistry to quantify the spatial distribution of electrons within molecules. Introduced by Becke and Edgecombe in 1990 [34]. ELF provides insights into the nature of chemical bonding, electron pair localization, and regions of high electron density in molecular systems, and the ELF value at a specific point in a molecule indicates the probability of finding an electron pair at that point. It is particularly useful for analyzing molecular structures with complex bonding patterns or investigating weak interactions like hydrogen bonding [35]. ELF is derived from the electron density and its gradient, utilizing quantum mechanical calculations, often based on density functional theory (DFT) [36, 37]

The topological analyses of the ELF, η(r) were carried out with the Multiwfn_3.7 program [38], and the graphical representations were visualized by the Chimera 1.16 program [39].

3 Results and interpretation

3.1 Analysis of reactivity by global descriptors

In a first step, the nature of the mechanism of these reactions is analyzed using global reactivity indices. These indices are effective tools that have been successfully used in many studies focused on Diels–Alder and [3 + 2] cycloaddition reactions to understand the reactivity of molecules to their ground state.

The values of the global reactivity indices, which are the electronic chemical potential (μ), the chemical hardness (η), the global electrophilicity (ω) and the nucleophilicity (N), of the reactants involved in these reactions are given in Table 1.

Table 1 B3LYP/6-31G(d) energies of the HOMO and LUMO in eV, electronic chemical potential μ, hardness η, electrophilic index ω and nucleophilic index N in eV of **I**a-c and **II**(*X* = O, NH and S)

	E_{HOMO}	E_{LUMO}	μ	η	Ω	N
Ia (R = H)	− 6.89	− 2.39	− 4.63	4.47	2.39	2.22
Ib (R = Me)	− 6.70	− 2.32	− 4.51	4.38	2.32	2.41
Ic (R = MeO)	− 6.42	− 2.16	− 4.31	4.23	2.20	2.69
II (X = S)	− 5.53	− 0.29	− 2.91	5.24	0.80	3.58
II (X = O)	− 5.34	− 0.40	− 2.84	4.94	0.83	3.78
II (X = NH)	− 5.04	− 0.54	− 2.79	4.50	0.86	4.08

Table 1 shows that the electronic chemical potential of **II** (X = O, NH, S) is always the largest, thus confirming that during these reactions, a charge transfer (CT) takes place from **II** (X = O, N, S) to **1**a-c, and this result is in good agreement with the computed CT analysis at the transition states (see later).

The electrophilic index of **I** a-c is higher than that of **II** (X = O, NH, S). On the other hand, the electrophilic values ω favor the electrophilic character for **II** a-c compounds, while compounds **II** (X = O, NH, S) behave as nucleophiles.

Reagents **I** a-c possess an electrophilicity index ω of 2.20 to 2.39 eV, being classified as borderline moderate and strong electrophiles based on the electrophilicity scale.[20]. In addition, reagents **II** (X = S, O and NH) have a nucleophilicity index N of 3.58 eV, 3.78 eV and 4.08 eV, respectively, which allow us to classify them as strong nucleophiles on the basis of the scale of nucleophilicity [32]. The introduction of the electron-releasing methyl and methoxy groups slightly decreases the electrophilicity of **I**-b and **I**-c and slightly improves the nucleophilicity, while the methyl and methoxy groups do not change the electrophilicity of **I**a-c. On the other hand, the heteroatomic substitution of X = S in **II** by X = O and X = NH slightly increases their nucleophilicity, and the reagent **II** (X = NH) is the most nucleophilic among these heteroatoms due to its higher electron density and lower electronegativity (see Table 1).

Therefore, since reactants **II** (X = S, O and NH) are strong nucleophiles and **II** a-c are strong electrophiles, the corresponding reactions are therefore expected to have strong polar characters.

3.2 Reactivity analysis by local descriptors

According to Domingo's polar model [40], the static indices of local electrophilicity ω_k ($\omega_k = \omega f_k^+$) [41] and local nucleophilicity N_k ($N_k = N f_k^-$) [42] are reliable descriptors for the prediction of the most favored electrophilic-nucleophilic interaction for the formation of a chemical bond between two atoms. It takes place between the most electrophilic site (characterized by the greatest value of ω_k) of the electrophilic molecule and the most nucleophilic site (characterized by the greatest value of N_k) of the nucleophilic molecule. The values of local electrophilicity ω_k for the reactive atoms of **I**a-c and of local nucleophilicity N_k of the reactive atoms of **II**(X = O, NH and S) calculated with the population analyzes NPA (Natural Population Analysis) and MPA (Mulliken Population Analysis) by the DFT/B3LYP 6-31G (d) method are reported in Table 2. The spurious negative values for f + with NPA have been commented by Toro-Labbé and Ayers [refs] underlining the association of orbital relaxation effects and nodal surfaces of the frontier orbitals [43, 44].

Table 2 Fukui index (f_k^+ and f_k^-) and values of local electrophilicity ωk for the reactive atoms of **I**a-c and of local nucleophilicity N_k for the reactive atoms of **II**(X = O, N and S) calculated by population analyzes NPA, MK

	Atom	MPA				NPA			
		f^+	f^-	ω_k	N_k	f^+	f^-	ω_k	N_k
Ia (R = H)	C2	0.06	/	0.15		0.07	0.18		
	C4	0.01		0.03		− 0.01	− 0.02		
Ib (R = Me)	C2	0.06		1.54		0.07	/	0.18	
	C4	0.01		0.02		− 0.01	0.02		
Ic (R = MeO)	C2	0.06		0.14		0.07	0.15		
	C4	0.01		0.02		− 0.01	0.02		
II (X = O)	N6	/	0.12		0.48	/	0.19		0.74
	O9		0.07		0.26		0.07		0.28
II (X = NH)	N6		0.02		0.09		0.13		0.53
	N9		0.02		0.09		0.13		0.53
II (X = S)	N6		0.13		0.48		0.13		0.47
	S9		0.13		0.47		0.09		0.34

The local nucleophilicity indices N_k for the reactive atoms of **II**(X = O, NH and S) and the local electrophilicity indices ω_k for the reactive atoms of **1**a-c show that the most favored interaction takes place between the N6 atom of **II** (X = O, NH and S) (having the highest value of N_k) and the C2 atom of **II**a-c (having the highest value of ω_k). Therefore, the formation of the N6-C2 bond observed experimentally [9] is correctly predicted by Domingo's polar model.

Recently, from an electronic point of view, Domingo and his co-workers [30] proposed other local descriptors, the P_k^+ electrophilic and P_k^- nucleophilic Parr functions, which are derived from the change in spin electron density that occurs during the GEDT process from the nucleophile to the electrophile. This method has proven to be a powerful tool in the study of local reactivity in polar processes. Therefore, in order to predict the most favorable electrophile/nucleophile interaction in these reactions, the electrophilic functions of Parr P_k^+ of **I** a-c and the nucleophilic functions of Parr P_k^- of **II**(X = O, N and S) were analyzed. The 3D representations of the Mulliken atomic spin density (ASD) of the radical cations $\mathbf{I}^+$ a-c and the radical anions $\mathbf{II}^-$ (X = O, NH and S), as well as the Parr nucleophilic functions P_k^- of **II**(X = O, NH and S) and the Parr P_k^+ electrophilic functions of **I** a-c are given in Fig. 1.

The analysis of the nucleophilic Parr functions P_k^- of nucleophiles **II** (X = O, NH and S) indicates that they are mainly concentrated on the two atoms N6 and X9 (see Scheme 1 for the numbering of the atoms) whose center N6 being more than three times nucleophilic than the X9 center for o-aminophenol and o-aminothiophenol; $P_{N6}^- = 0.32$ and $P_{O9}^- = 0.10$ in **II**(X = O), and $P_{N6}^- = 0.376$ and $P_{S9}^- = 0.024$ in **II**(X = S), while the nucleophilic Parr function of nitrogen N6 in o-phenylenediamine **II**(X = NH) $P_{N6}^- = 0.21$. On the other hand, the analysis of the P_k^+ electrophilic Parr functions of **I** a-c indicates that the C2 carbon atom is the most electrophilic center in these molecules, $P_{C2}^+ = 0.09$, 0.09 and 0.09 for **I**a(R = H), **I**b(R = CH3) and **I**c (R = OCH3), respectively, whereas the C4 carbon atom is not an electrophilic center $P_{C4}^+ = -0.03$ (**I**a), − 0.03 (**I**b) and − 0.03 (**I**c).

Consequently, the favorable electrophilic/nucleophilic interaction of these reactions of **I** a-c with **II**(X = O, NH and S) will take place between the most nucleophilic center of the **II**(X = O, NH and S) which is the nitrogen N6 and the most electrophilic center of **I** a-c which is the C2 carbon leading to the formation of C2-N6 bond before the C4-X9 bond, in good agreement with the experimental results.

3.3 Reactivity analysis by the dual descriptor

The spin densities of the N + 1/N-1 systems have been shown to be good approximations for the nucleophilic and electrophilic Fukui functions. Thus, the dual descriptor was calculated by difference between the spin densities of the N + 1/N-1 systems. In all representations of the dual descriptor, isodensity maps areas where descriptor values are negative ($\Delta f(r) < 0$) are red colored, whereas areas where descriptor values are positive ($\Delta f(r) > 0$) are colored in green.

The use of the dual descriptor $\Delta f(r)$ allows unambiguous prediction of the most reactive site with respect to an electrophilic or nucleophilic attack. Figure 2 represents the isodensity map of the dual descriptor for reactants **I** a-c and **II** (X = O, NH and S) for the first reaction of condensation, on which it can be observed that the carbon C2 in the three reactants **I** a-c has an electrophilic character ($\Delta f(r) > 0$, colored in green), and therefore, will react preferentially with nucleophiles, such as nitrogen N6 of **II**(X = O, NH and S).

The dual descriptors for the reagents **III** a-c (X = O, NH and S) calculated at the B3LYP/6-31G* level are displayed in Table 3, and electronic interaction is also observed between C4 and X9. The hetero atom X9 displays

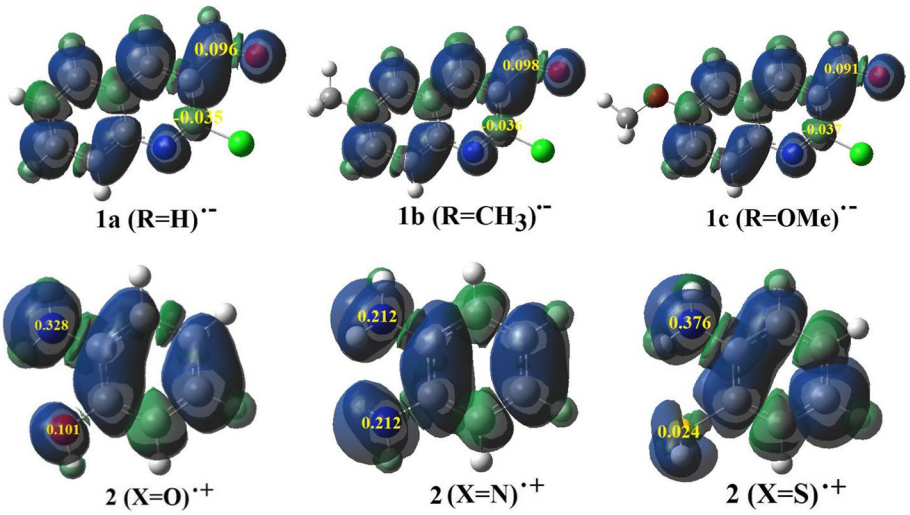

Fig. 1 3D representations of the ASD of the radical cation **2**(X = O, N, S)$^{\bullet+}$ and the radical anion **1**a-c$^{\bullet-}$, as well as the nucleophilic and electrophilic Parr functions of **2**(X = O,N and S) and **1**a-c

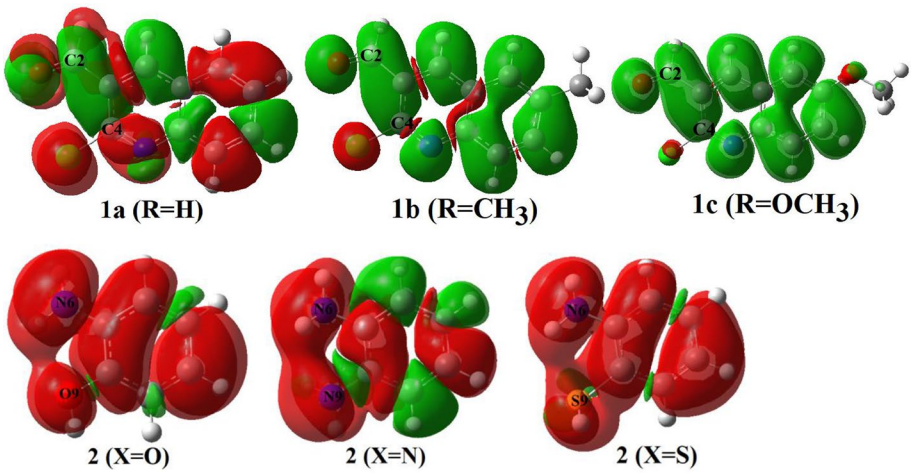

Fig. 2 The isodensity map of the dual descriptor $\Delta f(r)$ calculated for reactants 1a-c and 2(X = O, N, S), $\Delta f(r) > 0$ colored in green and $\Delta f(r) < 0$ colored in red

Table 3 Dual descriptor Δf or the reactive atoms of **III**a-c (X = O, N and S) calculated by population analyzes NPA, MPA

		MPA Δf	NPA Δf
IIIa (X = O)	C4	0.00	0.01
	O9	−0.06	−0.07
IIIb (X = O)	C4	0.00	0.01
	O9	−0.06	−0.07
IIIc (X = O)	C4	0.00	0.01
	O9	−0.05	−0.06
IIIa (X = NH)	C4	0.01	0.01
	N9	−0.09	−0.13
IIIb (X = NH)	C4	0.00	0.01
	N9	−0.08	−0.13
IIIc (X = NH)	C4	0.00	0.01
	N9	−0.07	−0.11
IIIa (X = S)	C4	0.00	0.01
	S9	−0.16	−0.24
IIIb (X = S)	C4	0.00	0.01
	S9	−0.15	−0.18
IIIc (X = S)	C4	0.00	0.01
	S9	−0.13	−0.16

a nucleophilic chemical behavior ($\Delta f < 0$), while C4 exhibits an electrophilic character ($\Delta f > 0$) in the all reagents,.

3.4 Energy aspect

The condensation of substituted 2-chloroquinoline-3-carbaldehydes (Ia-c) with o-aminophenol (II, X = O), o-aminothiophenol (II, X = S) and o-phenylenediamine (II, X = NH) to yield imines IV a-c is a stepwise reaction. The proposed reaction mechanism is a three-step mechanism, schematized in Scheme 2. The 2-chloroquinoline-3-carbaldehydes (Ia-c) protonated at carbonylic site leads to the reactants cationic intermediate I-1a-c in acid–base equilibrium with the Ia-c. In the following nucleophilic addition of one of the latter to C2 of I-1a-c, the most favorable geometry is with the angle between the aromatic substitution of amine and carbonyl oxygen amounting 180°, to get finally the imine in a Z configuration. Following that, a proton transfer leads to the reactants intermediate amine IIIa-c. This step is associated with the TS1 transition state. Next, the water molecule is removed from IIIa-c., which leads to the final product V through the transitional state TS2.

The condensation is followed by an intramolecular aromatic nucleophilic substitution, which is cyclized with high yields leading to the products V a-c (X = O, S and NH).

An exhaustive exploration of the potential energy surface allowed us to determine the different transition structures. Relative thermodynamic data and kinetic data calculated with B3LYP are reported in supplementary material. An overview of the geometries obtained for the particular points of the reaction mechanism studies is reported in Fig. 3.

The results shows that in the reaction mechanism, the protonation of the I-a-c carbonyl exocyclic group is thermodynamically favored with a slight difference of stabilization of the I-1-b and I-1c compounds (R = Me, OMe) of about 2 kcal/mol.

In the second step, the nucleophilic addition of molecules II (X = O, NH, S) to C2 of I-1a-c followed by a proton transfer for the formation of intermediates IIIa-c (X = O, NH, S) remains the kinetically determining step, with free activation enthalpies $\Delta G^{\neq}$ = 34.10 kcal/mol at 40.90 kcal/mol. It is noted that the radical R has no effect on the thermodynamic quantities, whereas the substitution X has a remarkable effect. The compounds III a-c (X = O) are thermodynamically more stable compared to other reagents with 3–6 kcal/mol free enthalpy difference, while the formation of compounds III a-c (X = S) is slower ($\Delta G^{\neq}$ TS1a = 40.30 kcal/mol, $\Delta G^{\neq}$ TS1b = 40.90 kcal/mol, $\Delta G^{\neq}$ TS1c = 40.80 kcal/mol).

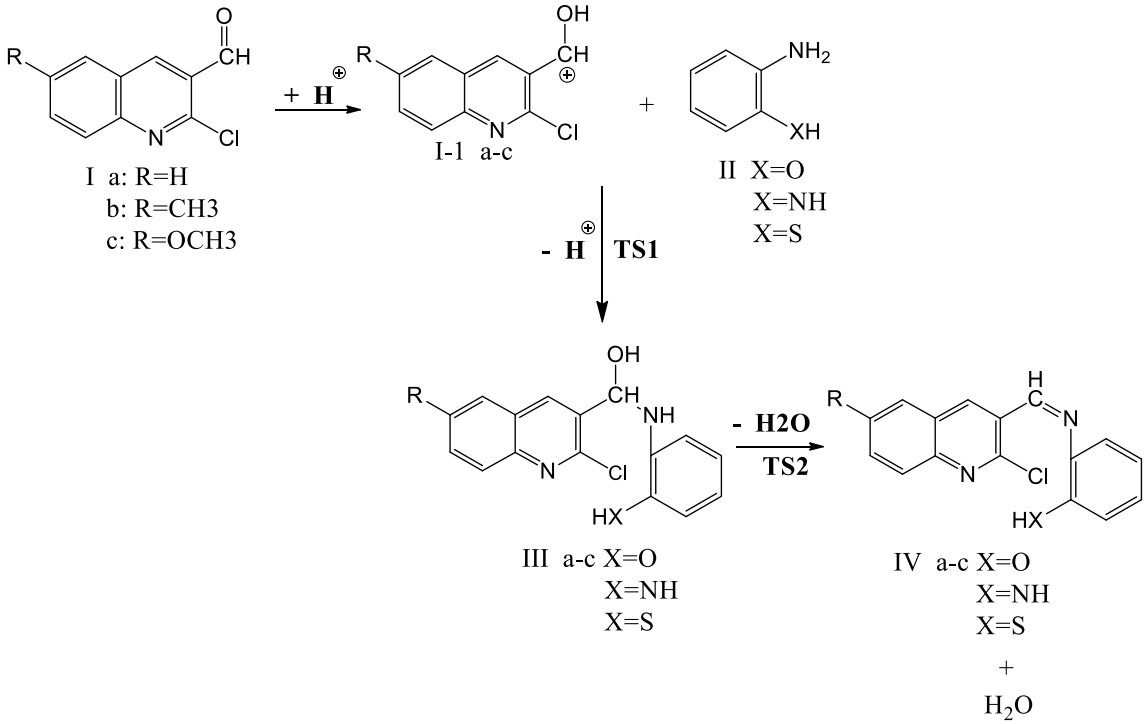

Scheme 2 The proposed reaction mechanism of the condensation of 2-chloroquinoline-3-carbaldehydes (Ia-c) with o-aminophenol (II, X = O), o-aminothiophenol (II, X = S) and o-phenylenediamine (II, X = NH)

Calculations show that the next step of removing a water molecule from the compounds III a-c(X = O, NH, S) is endothermic and spontaneous with a slight stabilization difference between IVa-c (X = NH) and IVa-c (X = S), and they are more stable compared to IVa-c (X = O) products by about 3 kcal/mol. It should be noted that the kinetic parameters of the IVa-c products (X = O, NH and S) are very close.

For the final products **V**a-c (X = O, NH and S), see Scheme 1, the intramolecular aromatic nucleophilic substitution of IVa-c (X = O, NH and S) is thermodynamically favored with significant stabilization of the products (**V**a-c, X = NH) with the enthalpy and free enthalpy energy difference (from about 5 kcal/mol up to 7 kcal/mol) compared to other products. The cyclization of the compounds IVa-c (X = NH) is the easiest with a difference of their activation energy decreased by 20 kcal relatively to other cycles.

In Fig. 3, the structures of the transition states corresponding to the formation of the cycles **V**a (X = O, NH and S) are illustrated with the distances of the new bonds and the charge transfer taking place from the nucleophile fragment **II** (X = O, NH and S) toward the electrophilic fragment **I**a, and the other structures of the transition are reported in supplementary material. From the analysis of the CT values, it is deduced that the formation of **Va-c**(X = S) has a considerable polar character with CT values amounting approximately 0.3e compared to the formation of other products, where their charge transfer lie between 0.0 up to 0.12e. Figure 4 graphically summarizes the evolution of the free enthalpy during the reaction.

3.4.1 Activation strain model ASM

The ASM [45] model, also named distortion/interaction model, has been introduced by Houk et al. [46–48] In this fragment approach, the activation energy is decomposed into two terms:

The first is the activation strain energy $\Delta E_{\text{strain}}(\zeta)$ which is related to required energy to the separate reactants deformation to reach the transition state structure. The second is the interaction energy $\Delta E_{\text{int}}(\zeta)$ which is the energy gain by the interaction between the deformed reactants:

$$\Delta E(\zeta) = \Delta E_{\text{int}}(\zeta) + \Delta E_{\text{strain}}(\zeta) \tag{10}$$

At the transition state, the activation energy is decomposed into the strain activation energy $\Delta E^{\ddagger}_{strain}$ and the interaction activation energy $\Delta E^{\ddagger}_{\text{int}}$ as follow:

$$\Delta E^{\ddagger} = \Delta E^{\ddagger}_{\text{int}} + \Delta E^{\ddagger}_{\text{strain}} \tag{11}$$

The interaction energy $\Delta E_{\text{int}}(\zeta)$ decomposition, between the deformed reactants, into its different terms has been proposed by Ziegler and Rauk [49] to allow a thorough evaluation of this interaction (see Eq. 12)

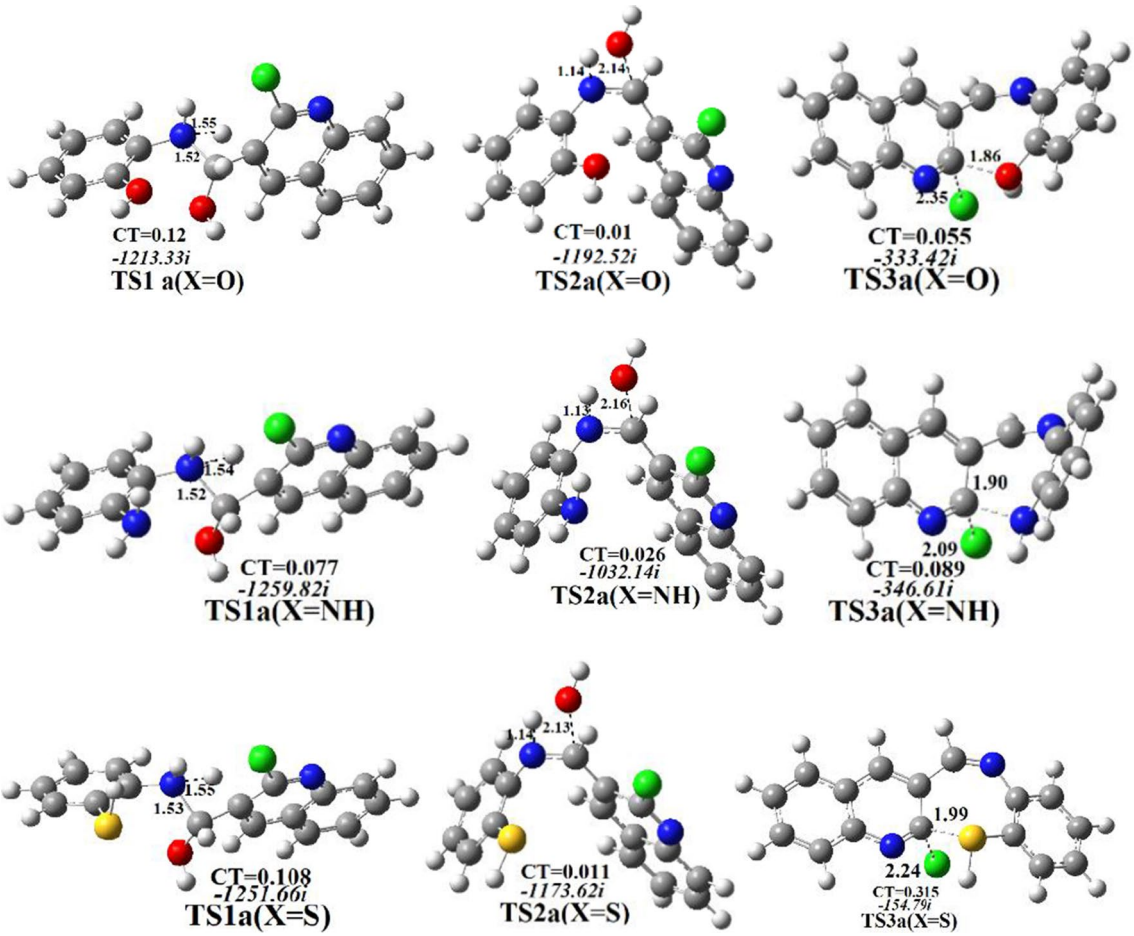

Fig. 3 B3LYP/6-31G(d) geometries of the TS a(X = O, NH,S) structures, (length in Angstroms Å, and charge transfer values in e)

$$\Delta E_{\text{int}}(\zeta) = \Delta V_{\text{elstat}}(\zeta) + \Delta E_{\text{Pauli}}(\zeta) + \Delta E_{\text{oi}}(\zeta) + \Delta E_{\text{disp}}(\zeta) \quad (12)$$

where, the term $\Delta V_{\text{elstat}}(\zeta)$ corresponds to the quasi-classical electrostatic interaction between the unperturbed charge distributions of the deformed reactants. Pauli repulsive orbital interaction $\Delta E_{\text{Pauli}}(\zeta)$ is responsible of the steric repulsion. As for the orbital interaction $\Delta E_{\text{oi}}(\zeta)$, it considers the charge transfer and polarization. Finally, $\Delta E_{\text{disp}}(\zeta)$ is the dispersion interaction energy [50–55].

The theoretical results for the first stage of the reactions showed that the variation of the substituent R (R = H, CH3, OCH3) has no effect on the energy, whereas the substitution of the X has a remarkable effect. In order to explain these results, the ASM/EDA analysis has been performed along the reaction coordinate. The ASM results indicate that the strain energy is the only factor controlling the kinetics of these reactions. The same observation was made for R = H, CH3, OCH3 and X = O, S (see Table 4).

Calculation results have already shown that the variation of X (with X = N, O and S) has a significant influence on the energy of these reactions. Therefore, the ASM analysis of the first stage of the reaction was performed for the R = H case, in order to understand the physical factors controlling the activation barrier heights. The ASM results comparison of the three reactions shows that the first step of the reaction where R = H and X = N (H-N reaction) is kinetically more favorable. ASM results of the H-N and H–O reactions (see Table 5) indicates that H-N reaction is favored by its low strain energy (E strain (H-N) = 35.3 kcal/mol *vs* E strain (H–O) = 39.03 kcal/mol). However, the strain energy of (R = H, X = N) and (R = H, X = S) reactions is almost identical (E strain (R = H, X = N) = 35.3 kcal/mol *vs* E strain (H–S) = 35.9 kcal/mol). The interaction energy is, then, the only factor controlling the activation barriers favoring the R = H, X = N reaction.

The nature of the interaction energy promoting of the H–N over H–O and H–S reactions is also analyzed using the EDA analysis. The EDA (Energy Decomposition Analysis) results at the transition state are noted in Table 6. These results show that the electrostatic stabilization (E elstat = − 147.91 kcal/mol) and orbital interaction

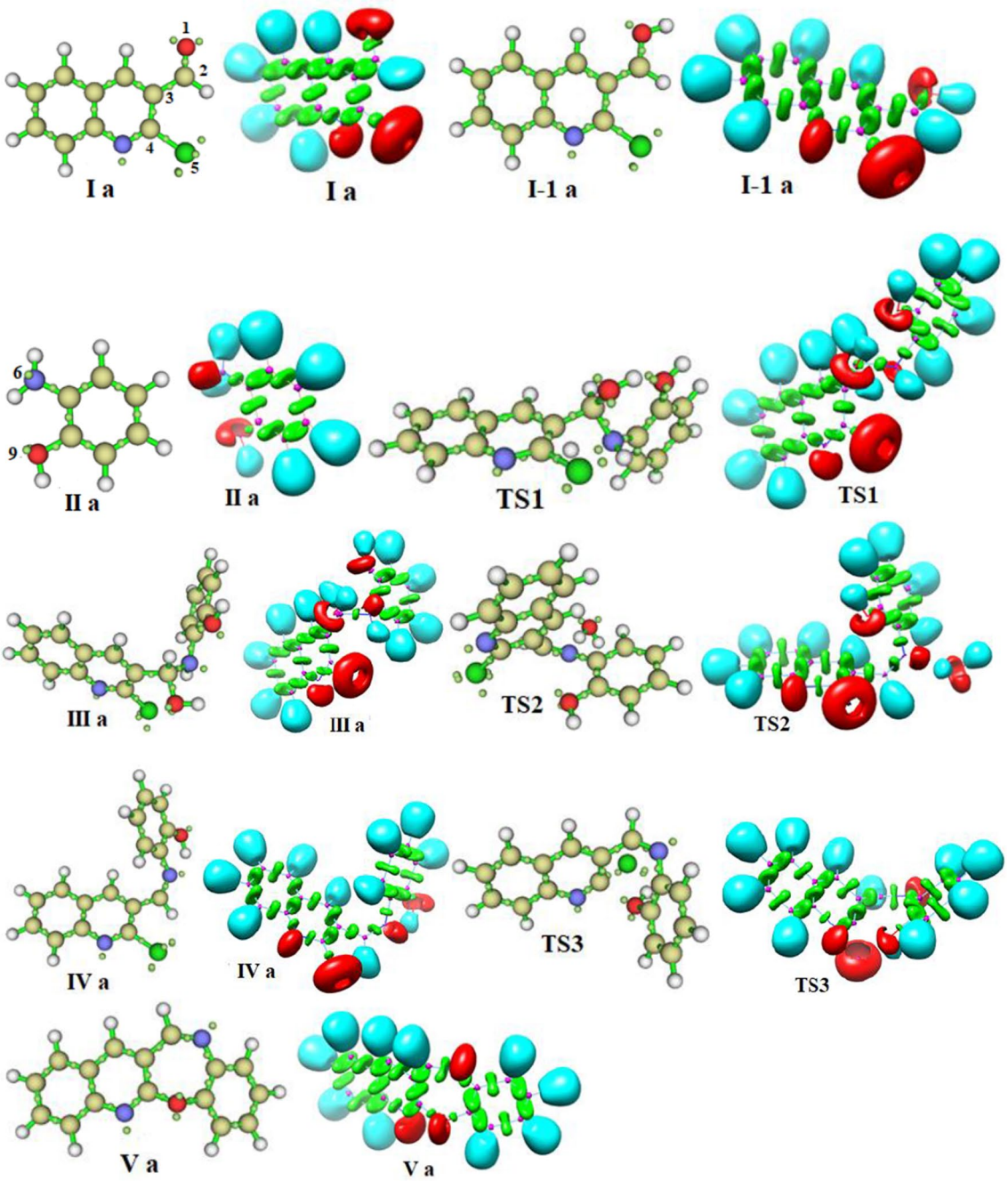

Fig. 4 ELF localization domains, represented with an isosurface value of ELF = 0.83 and basin attractor positions, monosynaptic basins are colored in red, di-synaptic basins are colored in green and protonated di-synaptic basins C–H and X–H are colored in blue

(E OI = − 195.22 kcal/mol) are the terms stabilizing the H-N reaction with respect to H–O and H–S reactions. Therefore, the strong Pauli repulsion was compensated by the electrostatic and orbital interaction stabilizations.

3.5 ELF topological analysis of the reaction path

To better understand the process of the formation of new N6-C2 and X9-C4 bonds along the reaction path of the

Table 4 ASM energies at the transition state given in kcal/mol for DA (decomposition analysis) reactions with (R = H, Me, OMe) and X = N

(a)	H–NH	Me–NH	OMe–NH
E Strain	25.00	25.01	39.85
E Int	− 0.19	− 0.01	− 15.62
Δ*E*	24.81	25.00	24.23
(b)	H–O	Me-O	OMe-O
E Strain	39.03	36.99	37.05
E Int	− 12.58	− 13.13	− 13.23
Δ*E*	26.44	23.86	23.83
(c)	H–S	Me-S	OMe-S
E Strain	35.93	35.82	35.90
E Int	− 11.85	− 11.83	− 11.73
Δ*E*	24.07	24.00	24.17

The ASM relative energies are calculated with respect to the pre-reactive energies

Table 5 ASM energies at the transition state given in kcal/mol for DA (decomposition analysis) reactions with R = H and X = , N, O and S

	H–N	H–O	H–S
E Strain	35.28	39.03	35.93
E Int	− 13.27	− 12.58	− 11.85
ΔE	22.01	26.44	24.07

The ASM relative energies are calculated with respect to the pre-reactive energies

Table 6 Interaction energies at the transition state given in kcal/mol for the H–N, H–O and H–S reactions

	H–N	H–O	H–S
E Pauli	331.66	319.37	319.44
E Elstat	− 147.91	− 141.60	− 140.68
E OI	− 195.22	− 187.43	− 186.68
E disp	− 3.78	− 3.66	− 4.03

cycloaddition reaction of 2-chloro-3-formylquinoline **1**a and o-aminophenol (**2**, X = O), we carried out an ELF (Electron Localization Function) analysis of stationary points. The populations of the most significant valence basins (those associated with regions involved in bond formation in this reaction), among other important parameters, ELF topological characteristics of separate reactants and selected points are shown in Table 7, while the corresponding positions of the ELF basin attractors are shown in Fig. 5.

As shown in Fig. 5, the Electron Localization Function (ELF) domains are represented with an isosurface value of ELF = 0.83. The colors of the basins are the following:

- monosynaptic basins V (X) correspond to non-bonded regions (which, in Lewis representation, indicates a lone pair of electrons) appear in red color.—di-synaptic basins V(X, Y) are found in bonding regions (C–C and C–X) appear in green color—protonated di-synaptic basins C–H and X–H appear in blue color. Purple points represent atoms.

- **At reactant point Ia,** the two monosynaptic basins V(O1), V'(O1) corresponds to the non-bonding pair of the oxygen atom O1 with a total population equal to 5.18e. For the chlorine atom Cl5 which binds with carbon C4, where chlorine has three monosynaptic basins V(Cl5), V'(Cl5) and V''(Cl5) corresponding to the non-bonding pair of the chlorine atom with 6.21e of a total population, the number of these basins will be increased to 6 basins during the reaction due to the increase in unbound electrons, this indicates the separation of chlorine from the carbon C4 (the breaking of the C4–Cl5 bond). The two di-synaptic basins V(C2-O1) and V(C4-Cl5) corresponding to the C2=O1 and C4-Cl5 bonds have electronic populations of 2.37e and 1.43e, respectively, and they will disappear during the reaction following the bonds breaking between these atoms.
- **At reactant point II (X = O),** the nitrogen atom N6 has a monosynaptic basin with an electron population of 1.9e. The two monosynaptic basins V(O9), V'(O9) correspond to the non-bonding pair of the oxygen atom O9 with 4.65e a total population. During the reaction, the number of these monosynaptic basins increases due to the dehydrogenation of oxygen and then, they will disappear due to the formation of the O9-C4 bond.
- **At reactant point I-1a,** we notice a decrease in the population of the di-synaptic basin V(O1-C2) from 2.387e to 1.78e, and it continues to decrease gradually in the other compounds until they completely disappear at TS2. The decrease in the number of monosynaptic basins V(O1)

Table 7 ELF valence basin populations of the selected points of the IRC directly involved in the formation of the N6–C2 and C4–O9 of reaction of **I**a-c with **II**(X = O, N and S). Distances are given in angstroms, Å

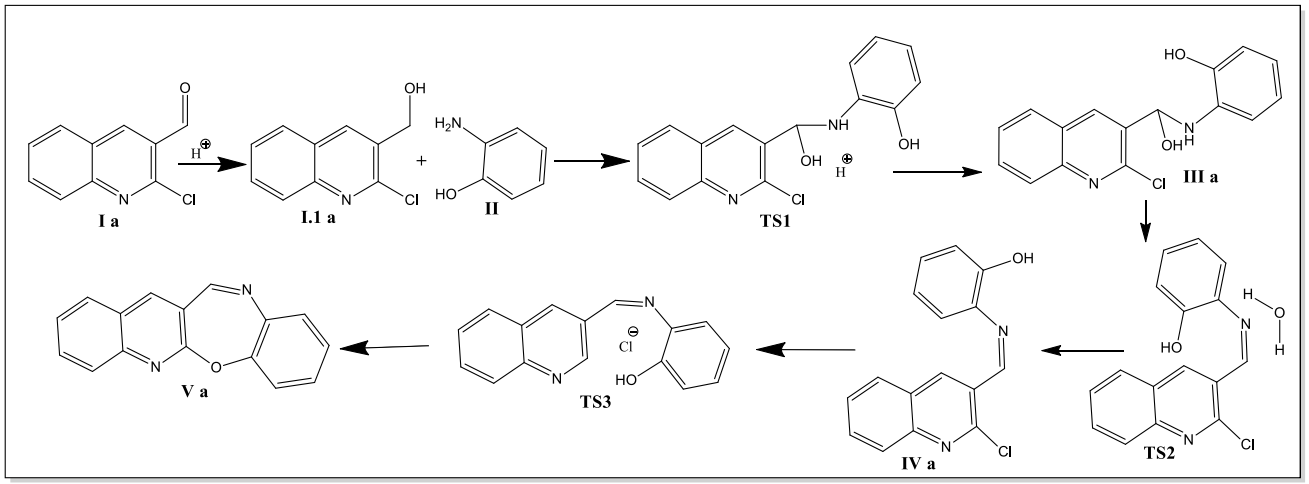

	I a and II	I.1 a	TS1	III a	TS2	IV a	TS3	V a
d (C2–N6)	–	–	1.52	146	1.33	1.28	1.28	1.28
d (C4–O9)	–	–	–	–	–	–	–	1.37
V(O1,C2)	2.37	1.78	1.39	1.29	–	–	–	–
V(C4,Cl5)	1.43	1.52	1.54	1.43	1.44	1.44	–	–
V(O1)	2.60	4.05	2.40	2.44	2.51	–		–
V ‘(O1)	2.58	–	2.28	2.39	2.24	–	–	–
V(C4)	–	–	–	–	–	–	0.52	–
V(Cl5)	2.70	2.80	3.04	3.13	3.00	3.04	1.25	–
V’(Cl5)	3.34	3.51	3.26	3.12	3.23	3.21	2.90	–
V’’(Cl5)	0.17	3.51	3.26	0.13	0.15	0.12	3.34	–
V(Cl5)	–	–	–	3.13	3.00	3.21	3.34	–
V(Cl5)	–	–	–	3.12	3.23	3.04	1.25	–
V(Cl5)	–	–	–	–	–	–	2.90	–
V(C2,N6)	–	–	1.80	1.67	2.97……	2.99	2.96	2.97
V(C4,O9)	–	–	–	–	–	–	–	1.42
V(O9,H)	1.61	–	1.62	1.62	1.62	1.65	1.83	–
V(N6)	1.90	–	1.77	1.94	–	2.60	2.64	2.56
V(O9)	2.33	–	2.30	2.22	2.41	2.03	1.24	2.69
V’(O9)	2.32	–	2.21	2.42	2.21	2.56	2.96	2.09
V’(O9)	–	–	0.13	–	–	–	–	–

from two to one basin and their population from 5.18e to 4.05e is due to the protonation of oxygen.

- **At transition state TS1,** the first remarkable topological change along the reaction path takes place, and a new dis-synaptic basin V (N6-C2) is created with an initial population of 1.80e. This relevant topological change indicates that the formation of the first N6-C2 bond begins to take place at a distance of 1.52 Å by the coupling of N6-to-C2.
- **At intermediate point IIIa,** the intermediate state in which the nucleophile factor attacks the reactive substance, when the nucleophile factor is partially associated with the central carbon atom carrying the outgoing group, while the outgoing atom remains partially connected to the central carbon atom.
- **At the transition state TS2,** the disappearance of the di-synaptic basin V(C2-O1) leading to the breaking of C2−O1 bond.
- **At the product point IVa,** the increase in the N value of dis-synaptic basin V (N6-C2) during the reaction up to 2.99e indicates the increase in the strength of the bond until it becomes a double bond after the release of water

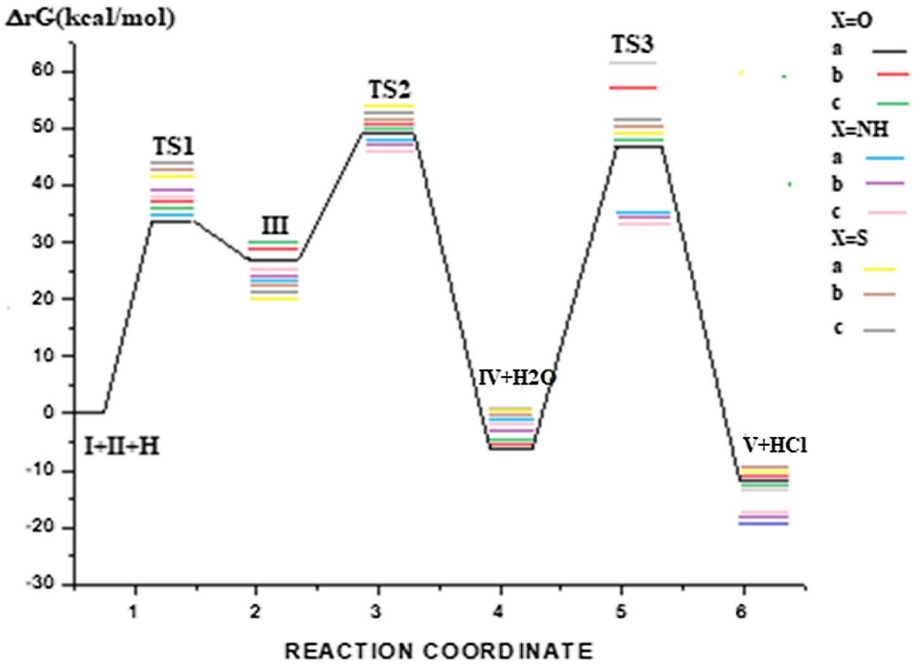

Fig. 5 Evolution of the free enthalpy during the reaction mechanism

at the compound level. We observe the disappearance of the monosynaptic basins of: oxygen O1.

- **At the transition state TS3,** the di-synaptic basin V(C4-Cl5) disappears, coinciding with the appearance of a new monosynaptic basin V(C4). This corresponds to the rupture of the C4-Cl5 bond.
- **At the final product 4(a, X = O), d (C2 = N6) = 1.28 Å and d(C4-O9) = 1.37 Å,** the appearance of the di-synaptic basin V(C4-O9) integrating a 1.42e population is indicative of C4-O9 bond formation. This is concomitant to the disappearance of di-synaptic basin V(O9,H) and the monosynaptic basins of Cl5 and C4 leading to the breaking of O9-H bond.

4 Conclusion

In this work, we brought theoretical elements giving light on the reactional mechanisms of the synthesis of benzo/oxa/thia/dia/zepines fused with quinoline, leading to a better understanding of the factors controlling the reaction. For the purpose, we used tools based on the conceptual density functional theory in connection with calculations of the energy and the electronic structure of the molecular systems. The evolution of electron density along the reaction path was performed by topological analysis with the electron localization function (ELF). The dual descriptor of chemical reactivity provided valuable information relating to the influence of electronic effects on the reactivity.

The analysis of the global reactivity indices indicates that **2**(X = O, N, S) are classified as good nucleophiles and **1**a-c as good electrophiles, thus suggesting a strong polar character of these reactions, a point confirmed by the high values of the computed charge transfer at the corresponding TS.

The analysis of the local reactivity indices of Fukui and Parr functions reveals that the most favorable interaction between the reactive centers along these polar reactions will take place between the most nucleophilic center of the **2** (X = O, N, S), namely the nitrogen N6 and the most electrophilic center of **1** a-c, which is carbon C2, same results obtained by the dual descriptor analysis.

In the energy point of view, the R substituent has no effect on the thermodynamic quantities, whereas the substituted X has a remarkable effect especially in the cyclization of the final products **V**, the products (**V**a-c, X = N) are the most stable and their cyclization is the easiest. In order to understand the physical factors controlling the kinetics of the first step of these reactions, ASM/EDA calculations have been performed. ASM results obtained for the substituent R variations indicate that the strain energy is the only factor controlling activation barriers heights. In addition, the ASM result shows that the variation of R influences on Estrain and Eint so as to have an identical activation energy, indicating that R has no influence on the energy. On the other hand, in the case of the substituent X variation, the Eint controls the kinetics of the cycloaddition reactions. The decomposition of interaction energy into its different terms indicates that the orbital interaction and electrostatic stabilization are the principal factors favoring the reaction R = H, X = N.

The ELF topological analysis of the formation of the two new bonds of the reaction path d(C2 = N6) = 1.28 Å and d(C4-O9) = 1.37 Å with electronic populations 2.99e and

1.42e, respectively, the bond rupture and bond formation along these reactions are non-concerted, allowing the exclusion of a pericyclic mechanism for these reactions.

Supplementary Information The online version contains supplementary material available at https://doi.org/10.1007/s00214-023-03052-2.

Author Contributions Conceptualization and methodology**:** were contributed by NB, HM, LM and CM. Investigation was contributed by NB, HM, NL, and HC. Writing—original draft preparation, was contributed by HM. Writing—review & editing, was contributed by CM, LM, HM. Experimental measurements were contributed by NB, NL, HM, AAM. Resources were contributed by NL and CM. Data curation was contributed by NB, HM, NL, LM, and HC. All authors have read and agreed to the published version of the manuscript.

Declarations

Conflict of Interest All authors have participated in (a) conception and design, or analysis and interpretation of the data; (b) drafting the article or revising it critically for important intellectual content; and (c) approval of the final version. The authors have no affiliation with any organization with a direct or indirect financial interest in the subject matter discussed in the manuscript.

References

1. Katritzky AR, Rees CW (1984) Comprehensive heterocyclic chemistry. Pergamon Press
2. Katritzky AR (1997) Advances in heterocyclic chemistry. Academic press
3. Balaban AT, Oniciu DC, Katritzky AR (2004) Aromaticity as a cornerstone of heterocyclic chemistry. Chem Rev 104:2777–2812. https://doi.org/10.1021/CR0306790
4. Pozharskii AF, Soldatenkov AT, Katritzky AR (2011) Heterocycles in Life and Society: An Introduction to Heterocyclic Chemistry, Biochemistry and Applications: Second Edition. Heterocycles Life Soc An Introd to Heterocycl Chem Biochem Appl Second Ed. https://doi.org/10.1002/9781119998372
5. Tsai M, Hong Y, Chang C et al (2007) 3-(9-Carbazolyl) carbazoles and 3, 6-Di (9-carbazolyl) carbazoles as effective host materials for efficient blue organic electrophosphorescence. Adv Mater 19:862–866
6. Hu Z-J, Yang J-X, Tian Y-P et al (2007) Synthesis and optical properties of two 2, 2′: 6′, 2 ″-terpyridyl-based two-photon initiators. J Mol Struct 839:50–57
7. Park S, Kwon O-H, Kim S et al (2005) Imidazole-based excited-state intramolecular proton-transfer materials: synthesis and amplified spontaneous emission from a large single crystal. J Am Chem Soc 127:10070–10074
8. Bhanumathi N, Rao KR, Sattur PB (1986) Novel formation of 11,12-dihydro-6H-quino[2,3-b] [1,5] benzodiazepines: reaction of 2-chloroquinoline-3-carbaldehydes with o-phenylenediamine. Heterocycles 24:1683–1685. https://doi.org/10.3987/R-1986-06-1683
9. Zecchini GP, Torrini I, Paradisi MP (1987) Synthesis of quino/2,3-b //1,5/ benzoxazepines: a novel tetracyclic ring system. Heterocycles 26:2443–2447. https://doi.org/10.3987/R-1987-09-2443
10. Torrini I, Zecchini GP, Paradisi MP (1988) The condensation products of 2-chloro-3-formylquinolines with o-aminothiophenol. Heterocycles (Sendai) 27:401–405
11. Nielsen FE, Pedersen EB (1985) Annulated 1,2,3-triazoles. 3. Synthesis of 1,2,3-triazolo[4,5-b][1,5]benzoxazepin-10(9H)-ones and 10-(4-substituted-1-piperazinyl)-1,2,3-triazolo[4,5-b][1,5] benzoxazepines. J Heterocycl Chem 22:1693–1701. https://doi.org/10.1002/JHET.5570220645
12. Becke AD (1993) Density-functional thermochemistry. III. The role of exact exchange. J Chem Phys 98:5648–5652. https://doi.org/10.1063/1.464913
13. Lee C, Yang W, Parr RG (1988) Development of the Colle-Salvetti correlation-energy formula into a functional of the electron density. Phys Rev B 37:785
14. Frisch MJ, Trucks GW, Schlegel HB et al (2009) Gaussian 09, rev. Gaussian Inc, Wallingford
15. Head-Gordon M, Pople JA (1988) A method for two-electron Gaussian integral and integral derivative evaluation using recurrence relations. J Chem Phys 89:5777–5786
16. Gonzalez C, Schlegel HB (1991) Improved algorithms for reaction path following: higher-order implicit algorithms. J Chem Phys 95:5853–5860
17. Fukui K, Yonezawa T, Nagata C, Shingu H (1954) Molecular orbital theory of orientation in aromatic, heteroaromatic, and other conjugated molecules. J Chem Phys 22:1433–1442
18. Fukui K (1970) Theory of orientation and stereoselection. In: Orientation and Stereoselection. Springer, pp 1–85
19. Parr RG, Szentpály LV, Liu S (1999) Electrophilicity index. J Am Chem Soc 121:1922–1924
20. Pérez P, Domingo LR, Aurell MJ, Contreras R (2003) Quantitative characterization of the global electrophilicity pattern of some reagents involved in 1, 3-dipolar cycloaddition reactions. Tetrahedron 59:3117–3125
21. Domingo LR, Arnó M, Contreras R, Pérez P (2002) Density functional theory study for the cycloaddition of 1, 3-butadienes with dimethyl acetylenedicarboxylate. Polar stepwise vs concerted mechanisms. J Phys Chem A 106:952–961
22. Parr RG, Yang W (1989) Density-functional theory of atoms and molecules Oxford Univ. Press. ed Oxford
23. Parr RG, Pearson RG (1983) Absolute hardness: companion parameter to absolute electronegativity. J Am Chem Soc 105:7512–7516
24. Chermette H (1999) Chemical reactivity indexes in density functional theory. J Comput Chem 20:129–154
25. Kohn W, Sham LJ (1965) Self-consistent equations including exchange and correlation effects. Phys Rev 140:A1133
26. Domingo LR, Chamorro E, Pérez P (2008) Understanding the reactivity of captodative ethylenes in polar cycloaddition reactions. A theoret study J Org Chem 73:4615–4624
27. Domingo LR, Pérez P (2011) The nucleophilicity N index in organic chemistry. Org Biomol Chem 9:7168–7175
28. Yang W, Mortier WJ (1986) The use of global and local molecular parameters for the analysis of the gas-phase basicity of amines. J Am Chem Soc 108:5708–5711
29. Chattaraj PK, Nath S, Sannigrahi AB (1994) Hardness, chemical potential, and valency profiles of molecules under internal rotations. J Phys Chem 98:9143–9145
30. Domingo LR, Pérez P, Sáez JA (2013) Understanding the local reactivity in polar organic reactions through electrophilic and nucleophilic Parr functions. RSC Adv 3:1486–1494
31. Chamorro E, Pérez P, Domingo LR (2013) On the nature of Parr functions to predict the most reactive sites along organic polar reactions. Chem Phys Lett 582:141–143
32. Ayers PW, Morell C, De Proft F, Geerlings P (2007) Understanding the Woodward-Hoffmann rules by using changes in electron density. Chem Eur J 13:8240–8247
33. Morell C, Grand A, Toro-Labbé A (2006) Theoretical support for using the Δf (r) descriptor. Chem Phys Lett 425:342–346
34. Becke AD, Edgecombe KE (1990) A simple measure of electron localization in atomic and molecular systems. J Chem Phys 92:5397–5403

35. Gatti C (2005) Chemical bonding in crystals: new directions. Zeitschrift für Krist Mater 220:399–457
36. Silvi B, Savin A (1994) Classification of chemical bonds based on topological analysis of electron localization functions. Nature 371:683–686
37. Savin A, Jepsen O, Flad J et al (1992) Electron localization in solid-state structures of the elements: the diamond structure. Angew Chemie Int Ed English 31:187–188
38. Lu T, Chen F (2012) Multiwfn: a multifunctional wavefunction analyzer. J Comput Chem 33:580–592
39. Pettersen EF, Goddard TD, Huang CC et al (2004) UCSF Chimera—A visualization system for exploratory research and analysis. J Comput Chem 25:1605–1612
40. Domingo LR, Aurell MJ, Pérez P, Contreras R (2002) Quantitative characterization of the local electrophilicity of organic molecules. Understanding the regioselectivity on Diels−Alder reactions. J Phys Chem A 106:6871–6875
41. Pérez P, Domingo LR, Duque-Noreña M, Chamorro E (2009) A condensed-to-atom nucleophilicity index. An application to the director effects on the electrophilic aromatic substitutions. J Mol Struct Theochem 895:86–91
42. Reed AE, Weinhold F (1983) Natural bond orbital analysis of near-Hartree-Fock water dimer. J Chem Phys 78:4066–4073. https://doi.org/10.1063/1.445134
43. Echegaray E, Cárdenas C, Rabi S et al (2013) In pursuit of negative Fukui functions: examples where the highest occupied molecular orbital fails to dominate the chemical reactivity. J Mol Model 19:2779–2783
44. Zamora PP, Bieger K, Cuchillo A et al (2021) Theoretical determination of a reaction intermediate: Fukui function analysis, dual reactivity descriptor and activation energy. J Mol Struct 1227:129369
45. Bickelhaupt M, Bickelhaupt M (1999) Understanding reactivity with Kohn–Sham molecular orbital theory: E2–S. J Comput Chem 20:114–128
46. Kelly TR, Hcnutt RW (1975) Cyclobutenone: the synthesis and Diels-Alder reactivity of 4,4-dimethylcyclobutenone. Tetrahedron Lett 4:285–288
47. Hamlin TA, Fernández I, Bickelhaupt FM (2019) How Dihalogens Catalyze Michael Addition Reactions. Angew Chemie - Int Ed 58:8922–8926. https://doi.org/10.1002/anie.201903196
48. Ess DH, Houk KN (2007) Distortion/interaction energy control of 1,3-dipolar cycloaddition reactivity. J Am Chem Soc 129:10646–10647. https://doi.org/10.1021/ja0734086
49. Ziegler T, Rauk A (1977) On the calculation of bonding energies by the Hartree Fock Slater method-I. The transition state method. Theor Chim Acta 46:1–10. https://doi.org/10.1007/BF02401406
50. Wolters LP, Bickelhaupt FM (2015) The activation strain model and molecular orbital theory. Wiley Interdiscip Rev Comput Mol Sci 5:324–343. https://doi.org/10.1002/wcms.1221
51. von Hopffgarten M, Frenking G (2012) Energy decomposition analysis. Wiley Interdiscip Rev Comput Mol Sci 2:43–62. https://doi.org/10.1002/wcms.71
52. Liu S, Lei Y, Qi X, Lan Y (2014) Reactivity for the Diels-Alder reaction of cumulenes: A distortion-interaction analysis along the reaction pathway. J Phys Chem A 118:2638–2645. https://doi.org/10.1021/jp411914u
53. Levandowski BJ, Hamlin TA, Bickelhaupt FM, Houk KN (2017) Role of orbital interactions and activation strain (distortion energies) on reactivities in the normal and inverse electron-demand cycloadditions of strained and unstrained cycloalkenes. J Org Chem 82:8668–8675. https://doi.org/10.1021/acs.joc.7b01673
54. Jin R, Liu S, Lan Y (2015) Distortion–interaction analysis along the reaction pathway to reveal the reactivity of the Alder-ene reaction of enes. RSC Adv 5:61426–61435. https://doi.org/10.1039/C5RA10345B
55. Fernández I, Bickelhaupt FM (2014) The activation strain model and molecular orbital theory: understanding and designing chemical reactions. Chem Soc Rev 43:4953–4967. https://doi.org/10.1017/CBO9780511544750.008